

# Towards Better Text-Image Consistency in Text-to-Image Generation

Zhaorui Tan,<sup>1</sup> Zihan Ye,<sup>1</sup> Xi Yang,<sup>1</sup> Qiufeng Wang,<sup>1</sup> Yuyao Yan,<sup>1</sup> Kaizhu Huang<sup>2\*</sup>

<sup>1</sup> Xi'an Jiaotong-Liverpool University

<sup>2</sup> Duke Kunshan University

{Zhaorui.Tan21, Zihan.Ye22}@student.xjtlu.edu.cn, {Xi.Yang01, qiufeng.wang}@xjtlu.edu.cn, joshuayyy@gmail.com, kaizhu.huang@dukekunshan.edu.cn

## Abstract

Generating consistent and high-quality images from given texts is essential for visual-language understanding. Although impressive results have been achieved in generating high-quality images, text-image consistency is still a major concern in existing GAN-based methods. Particularly, the most popular metric  $R$ -precision may not accurately reflect the text-image consistency, often resulting in very misleading semantics in the generated images. Albeit its significance, how to design a better text-image consistency metric surprisingly remains under-explored in the community. In this paper, we make a further step forward to develop a novel CLIP-based metric termed as Semantic Similarity Distance ( $SSD$ ), which is both theoretically founded from a distributional viewpoint and empirically verified on benchmark datasets. Benefiting from the proposed metric, we further design the Parallel Deep Fusion Generative Adversarial Networks (PDF-GAN), which can fuse semantic information at different granularities and capture accurate semantics. Equipped with two novel plug-and-play components: Hard-Negative Sentence Constructor and Semantic Projection, the proposed PDF-GAN can mitigate inconsistent semantics and bridge the text-image semantic gap. A series of experiments show that, as opposed to current state-of-the-art methods, our PDF-GAN can lead to significantly better text-image consistency while maintaining decent image quality on the CUB and COCO datasets.

## Introduction

Generating images from text descriptions, usually known as Text-to-Image Generation (T2I), is a challenging task that requires both generating high-quality images and maintaining text-image consistency. Although Generative Adversarial Networks (GANs) based methods (Yuan and Peng 2019; Hong et al. 2018; Li et al. 2020; Gou et al. 2020; Cheng et al. 2020; Ramesh et al. 2021; Tao et al. 2020) have achieved impressive results in generating high-quality images from text descriptions, they still struggle to keep the text-image consistency within complex semantics. Once the text descriptions become more complex, the semantics of the generated image will likely mismatch its text, although it comes with a high-quality score. Thus, the measurement of text-image consistency remains a critical concern in T2I generation.

Albeit its significance, how to design a better text-image consistency metric surprisingly remains under-explored in

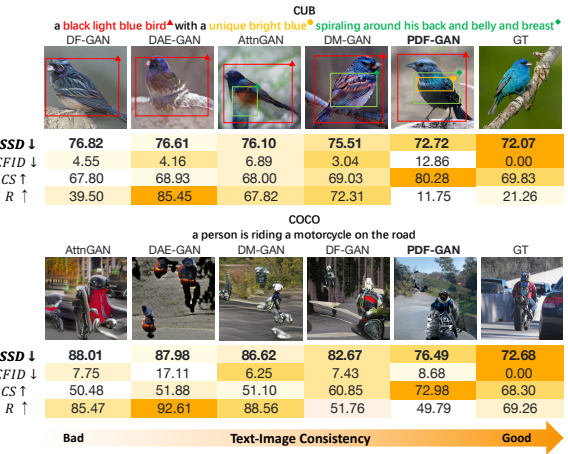


Figure 1: Illustration of synthesized images with CFID, CS, and  $SSD$  score for Attn-GAN, DM-GAN, DAE-GAN, DF-GAN, and our PDF-GAN. Better metric scores are highlighted with higher saturation.  $SSD$  demonstrates much better text-image consistency than  $R$ , CS and CFID.

the community. To illustrate it clearly, we conduct a simple experiment for current potential text-image consistency metrics in Fig. 1.<sup>1</sup>

The most widely used T2I synthesis metric,  $R$ -precision ( $R$ ) (Xu et al. 2018), judges text-image consistency by evaluating if the generated image is more consistent with the given text than the other 99 randomly sampled texts. Such a measure may not accurately reflect the direct consistency between texts and images. The right-most column of Fig. 1 shows that the  $R$  score on ground truth (GT) is even seriously worse than synthetic images.<sup>2</sup> It results in very misleading semantics in the generated image. As highlighted by rectangles in Fig. 1, DAE-GAN achieves the highest  $R$ , but still produces very text-inconsistent images. Meanwhile, random sampling may also be highly biased by datasets. The more significant variation between the sampled texts

<sup>1</sup>  $SSD$ , CS and CFID in this paper are scaled by 100 for better readability. SOA is omitted since it cannot be applied to CUB.

<sup>2</sup> We use the 99 random samples that can reproduce the  $R$  in AttnGAN (Xu et al. 2018) to calculate  $R$  on GT pairs.

\*Corresponding author

and the given descriptions leads to significantly better scores on more diverse datasets (i.e., COCO (Lin et al. 2014) v.s. CUB (Wah et al. 2011) in Fig. 1 (R)). Semantic Object Accuracy (SOA) (Hinz, Heinrich, and Wermter 2020), one recently-proposed metric specifically designed for evaluating multi-object text-image consistency, would still fail to measure the entire semantic consistency without evaluating object attributes and relationships. More seriously, SOA cannot be applied to datasets where only one object usually appears in the generated images, such as CUB. To alleviate these issues, researchers have to rely on Human Evaluation (Tao et al. 2020). However, the process is usually costly, and its settings vary a lot among different methods, making it harder to apply in practical scenarios.

In this work, we make a further step forward and propose a novel CLIP-based text-image consistency metric from a distributional viewpoint, termed Semantic Similarity Distance (*SSD*). For T2I synthesis tasks, CLIP offers a joint language-vision embedding space where the similarity between semantic distributions of images and text can be directly measured. Our *SSD* is designed by combining two terms: 1) the first-moment term measures directly the text-image semantic similarity, reflecting the semantic bias between generated images and texts; 2) the second-moment term evaluates the difference of semantic variation between synthesized and real images conditioned on texts, suggesting that the diversity of semantics in the generated images should also be consistent with that of the real images. The second term can bring more credit to precise semantics, balancing the evaluation between overall and detailed consistency. Moreover, due to the large-scale pre-trained CLIP, *SSD* alleviates the bias in datasets and can be compared across different datasets.

On the theoretical front, we show that *SSD*’s rationale is rooted in using a modified Wasserstein Distance for measuring the divergence of two distributions. We also show that it can be closely linked with two recent metrics, CLIPScore (CS) (Hessel et al. 2021) and Conditional Frechet Inception Distanc (CFID) (Soloveitchik et al. 2021), but exhibits more desirable properties in measuring the semantic consistency. CS directly evaluates the similarity between images and texts’ CLIP (Radford et al. 2021) embeddings, merely accounting for the first term in *SSD*. As shown in Fig. 1, generated images may even achieve better CS than GT, partially showing its limitation as a metric. Meanwhile, we show that CFID inappropriately measures the distance between text-conditioned real and fake image distributions, which is seriously affected by semantic redundancies (i.e. the semantics not specified by given texts) in real images. Fig. 1 also illustrates its incapability of measuring text-image consistency.

With the benefits of *SSD*, there are two findings as follows: 1) Different levels of semantic information can significantly help with text-image consistency. However, the semantic gap will cause optimization conflicts between adversarial loss and semantic perceptual loss (Xu et al. 2018), as shown in Fig. 2 (a). As such, brutally adding semantic perceptual loss weakens the semantic supervision, leading to a sub-optimal performance in text-image consistency. 2) The mismatched samples for discrimination usually utilize

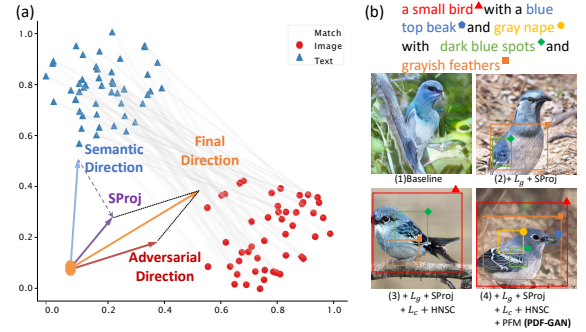


Figure 2: (a) T-SNE map of CLIP embeddings for randomly sampled GT text-image pairs in the CUB dataset. (b) Examples generated of different components are added.

shifted samples in a batch or random samples from other classes, which may lead to degradation of text-image consistency, especially in case of contrastive losses. According to the above findings, we propose a novel one-stage T2I generation framework named PDF-GAN as Fig. 3, consisting of Parallel Fusion Modules (PFMs) with semantic perceptual losses to fuse different-level granularity textual data. To further improve text-image consistency, we design two novel plug-and-play modules: Hard-Negative Sentence Constructor (HNSC) and Semantic Projection (SProj). HNSC constructs stable and controllable hard negative textural samples instead of sampling mismatched textual samples from the dataset to alleviate dataset bias. SProj constrains the optimization direction of semantic loss, projecting it to the direction that does not conflict with the adversarial loss to overcome the semantic gap. As Fig. 2 (b) shows, our PDF-GAN with HNSC and SProj significantly improves text-image consistency while maintaining decent image quality.

Our contributions are summarized threefold:

- We introduce a novel metric, Semantic Similarity Distance, which evaluates both text-image similarity and semantic variation difference between generated images and real images conditioned by the texts. *SSD* is theoretically well founded and can be cross-compared on different datasets.
- We propose a novel framework, Parallel Deep Fusion Generative Adversarial Networks (PDF-GAN), with semantic perceptual losses and PFMs to fuse semantic information at different levels.
- We design an HNSC that mines hard negative textual samples and SProj that alleviates the semantic gap and enhances text-image consistency.

## Related Work

**GANs for T2I** To improve the image quality and size in the first GAN-based approach (Reed et al. 2016), most methods adopt a multi-stage architecture for a coarse-to-fine generating process (Zhang et al. 2017, 2018; Wang et al. 2021; Bodla, Hua, and Chellappa 2018; Zhang, Xie, and Yang 2018; Gao et al. 2019; Huang, Wang, and Gong 2019; Xu et al. 2018; Zhu et al. 2019; Seshadri and Ravindran

2021). The attention mechanism (Xu et al. 2018; Huang, Da Xu, and Oppermann 2019; Ruan et al. 2021; Li et al. 2019) and extra networks (Ma, Zhang, and Zhang 2019; Tan et al. 2019; Cha, Gwon, and Kung 2019; Zhang et al. 2021; Qiao et al. 2019; Zhu et al. 2019; Seshadri and Ravindran 2021) are frequently applied to emphasize the semantics. DF-GAN (Tao et al. 2020) proposes a one-stage backbone with Deep Fusion Blocks using Affine and a one-way discriminator output with Matching-Aware Gradient Penalty. It avoids entanglements between generators without using the computationally expensive cross attention.

**Contrastive Language-Image Pre-training** CLIP (Radford et al. 2021) is a large-scale multi-modal pre-training model that maps images and language to a joint latent space, aligning them by maximizing their Cosine similarity. CLIP has been widely used as pre-trained encoders for T2I GAN-based models (Brock, Donahue, and Simonyan 2018; Gal et al. 2021), transformer-based generators (Wang et al. 2022), and diffusion models (Ramesh et al. 2022).

**Text-Image Consistency Metrics** Built upon the Cosine similarity between image and text embeddings, the widely-used metric  $R$  (Xu et al. 2018) evaluates if the generated image is more similar to the GT texts than random samples from the dataset.  $R$  does not measure directly the semantic consistency, which may be highly biased by the dataset. To this end, SOA (Hinz, Heinrich, and Wermter 2020) uses a pre-trained object detection model to evaluate whether an object mentioned by text exists in the generated image. Failing to measure the entire semantic consistency, SOA cannot be applied to datasets where only one object appears in the generated images (e.g. CUB). Owing to CLIP’s popularity, CS (Hessel et al. 2021) is designed for image captioning, yet Cosine similarity of CLIP embeddings may not explicitly bind attributes to objects and neglects semantic variations (Ramesh et al. 2022). With the conditional distribution, CFID (Soloveitchik et al. 2021) evaluates the distance between text-conditioned fake and real image distributions. However, directly aligning fake and real distributions may mismatch the redundant parts in real images, i.e. those contents not specified by texts. This severely affects CFID’s effect in measuring text-image consistency.

## Semantic Similarity Distance

In this section, we set out our novel metric for quantitatively evaluating T2I models. For better measuring the text-image consistency, our metric evaluates not only direct text-image semantic similarity but also the semantic variation difference between synthesized and real images conditioned on texts.

From a distributional perspective, we assume that normalized embeddings of generated image  $\tilde{e}_f$ , real image  $\tilde{e}_r$ , and text  $\tilde{e}_s$  distributions are all Gaussian-like distributions  $\Phi$  in a joint language-vision embedding space (CLIP Space):

$$\mathbb{Q}_f = \Phi(m_f, \mathbb{C}_{ff}), \mathbb{Q}_r = \Phi(m_r, \mathbb{C}_{rr}), \mathbb{Q}_s = \Phi(m_s, \mathbb{C}_{ss}),$$

where  $m$  and  $\mathbb{C}$  denote the mean and covariance;  $f$ ,  $r$  and  $s$  mean the generated images, real images, and texts, respectively. Conditioned on the same text  $s$ , the generated and real

images’s conditional distribution,  $\mathbb{Q}_{f|s}$ ,  $\mathbb{Q}_{r|s}$ , are given as:

$$\mathbb{Q}_{f|s} = \Phi(m_{f|s}, \mathbb{C}_{ff|s}), \mathbb{Q}_{r|s} = \Phi(m_{r|s}, \mathbb{C}_{rr|s}),$$

where  $\mathbb{C}_{ff|s}$  and  $\mathbb{C}_{rr|s}$  represent conditional covariances of  $\tilde{e}_f$  and  $\tilde{e}_r$  that are constant and independent of condition  $\tilde{e}_s$ . We are now ready to define our Semantic Similarity Distance.

**Definition 1.** As the ultimate goal is to measure the semantic distance among  $\tilde{e}_f$  and  $\tilde{e}_s$ , we consider the distance between  $\mathbb{Q}_f$ , and  $\mathbb{Q}_s$ , and the distance between  $\mathbb{Q}_{ff|s}$  and  $\mathbb{Q}_{rr|s}$ . Our  $SSD$  is then defined as follows:

$$SSD(\mathbb{Q}_f, \mathbb{Q}_s, \mathbb{Q}_{f|s}, \mathbb{Q}_{r|s}) = [1 - \cos(m_f, m_s)] + \|d(\mathbb{C}_{ff|s}) - d(\mathbb{C}_{rr|s})\|^2, \quad (1)$$

where  $d(\cdot)$  represents matrix’s the diagonal part.<sup>3</sup>

Since a pre-trained CLIP model is used to map the image and text to a joint language-vision embedding space, it is intuitive to measure their embeddings’ Cosine distance, as done in the first-moment term of Eq. (1). Due to the semantic gap between  $\mathbb{Q}_f$  and  $\mathbb{Q}_s$ , solely measuring the Cosine distance cannot fully reflect the distribution divergence. We then take  $\mathbb{Q}_{f|s}$  and  $\mathbb{Q}_{r|s}$  into consideration to bridge the semantic gap. We argue that if a model can fully capture semantics, its generated images should share the same semantic variation as the real images. Semantic variation can also help bind objects and attributes, leading to more precise semantic alignment. Note that we do not align  $\mathbb{Q}_{f|s}$  and  $\mathbb{Q}_{r|s}$  directly because it over-concerns the redundancies that are not described by the text. Therefore, we design a second-moment term in Eq. (1) to evaluate the semantic variation by calculating the diagonal differences between text conditioned covariance of fake and real image distributions.

Subsequently, we will support the plausibility of  $SSD$  by proving some lemmas.

**Lemma 1.** *If  $\mathbb{C}$  is a non-negative diagonal matrix, the second-moment term can be rewritten as:*

$$\|d(\mathbb{C}_{ff|s}) - d(\mathbb{C}_{rr|s})\|^2 \quad (2)$$

$$\begin{aligned} &\propto \text{Tr}[(\mathbb{C}_{ff|s}^{\frac{1}{2}} - \mathbb{C}_{ff|s}^{\frac{1}{2}})^2] \\ &= \text{Tr}[\mathbb{C}_{ff|s} + \mathbb{C}_{rr|s} - 2(\mathbb{C}_{ff|s}^{\frac{1}{2}} \mathbb{C}_{rr|s} \mathbb{C}_{ff|s}^{\frac{1}{2}})^{\frac{1}{2}}]. \end{aligned} \quad (3)$$

*Proof.* According to (Kay 1993), conditional covariances can be equivalently written as follows:

$$\mathbb{C}_{ff|s} = \mathbb{C}_{ff} - \mathbb{C}_{fs} \mathbb{C}_{ss}^{-1} \mathbb{C}_{sf}, \mathbb{C}_{rr|s} = \mathbb{C}_{rr} - \mathbb{C}_{rs} \mathbb{C}_{ss}^{-1} \mathbb{C}_{sr}.$$

Since  $\mathbb{C}_{**}$  is defined as a covariance matrix, which is a positive semi-definite matrix. Meanwhile, in CLIP space we only focus the diagonal part of  $\mathbb{C}$  because CLIP tries to maximize the Cosine similarity between embeddings via training. Thus  $\mathbb{C}$  can be simplified as a non-negative diagonal matrix.  $\square$

**Lemma 2.** *When  $m_f, m_s$  are normalized, the first-moment term can be rewritten as:*

$$1 - \cos(m_f, m_s) \triangleq \|m_f - m_s\|^2. \quad (4)$$

<sup>3</sup>We scale our  $SSD$  by 100 for better readability in this paper.

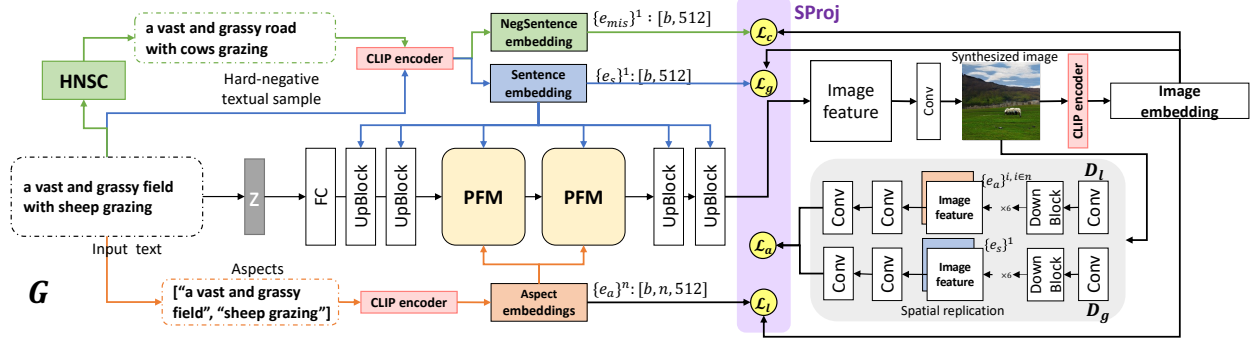


Figure 3: Overall Framework of PDF-GAN.

*Proof.* Cosine distance is equivalent to Euclidean distance of normalized vectors. In CLIP space,  $m_f, m_s$  are normalized embeddings of generated image  $\tilde{e}_f$  and text  $\tilde{e}_s$ .  $\square$

We now show how our  $SSD$  can be theoretically linked with the other metrics including CS and CFID in T2I synthesis, but exhibits more desirable characteristics.

**Proposition 1.** *If we only use the first term in Eq. (1), our  $SSD$  is converted to CLIP-Score (CS).*

*Proof.* The Cosine similarity term  $\cos(m_f, m_s)$  in Eq. (4) is equivalent to CS:

$$\begin{aligned} \cos(m_f, m_s) &= \mathbb{E} [\cos(\tilde{e}_f, \tilde{e}_s)] \\ &\propto \omega * \mathbb{E} [\max(\cos(\tilde{e}_f, \tilde{e}_s), 0)] \\ &= \text{CS}(\tilde{e}_f, \tilde{e}_s), \end{aligned}$$

where  $\omega$  is a constant scale-coefficient used in CS.  $\square$

**Proposition 2.** *If we measure the distance between  $m_{f|s}$  and  $m_{r|s}$  for the first term,  $SSD$  will be equivalent to Conditional Frechet Inception Distance (CFID).*

*Proof.* By Lemma 1 and 2,  $SSD$  can be rewritten as:

$$\begin{aligned} &\|m_f - m_s\|^2 + \\ &Tr[\mathbb{C}_{ff|s} + \mathbb{C}_{rr|s} - 2(\mathbb{C}_{ff|s}^{\frac{1}{2}} \mathbb{C}_{rr|s} \mathbb{C}_{ff|s}^{\frac{1}{2}})^{\frac{1}{2}}]. \end{aligned} \quad (5)$$

If we use  $m_{f|s}$  and  $m_{r|s}$  for the first term, we have:

$$\begin{aligned} &\|m_{f|s} - m_{r|s}\|^2 + \\ &Tr[\mathbb{C}_{ff|s} + \mathbb{C}_{rr|s} - 2(\mathbb{C}_{ff|s}^{\frac{1}{2}} \mathbb{C}_{rr|s} \mathbb{C}_{ff|s}^{\frac{1}{2}})^{\frac{1}{2}}] \\ &= \text{CFID}(\mathbb{Q}_{f|s}, \mathbb{Q}_{r|s}). \end{aligned} \quad (6)$$

Eq. (1) can be changed to CFID.  $\square$

Our new proposed  $SSD$  can be comprehended as evaluating direct consistency between text and images as a first-moment bias term and semantic variation difference between fake images and real images conditioned by text as a second-moment variation term. In contrast, CS omits the second-moment variation term, thus causing weakness in estimating semantic variations. CFID inappropriately considers the first-moment bias term as the difference between fake

and real image distributions, which may mismatch the redundancy contents in the images. Eq.(1) focuses on measuring primary semantic changes, bringing more consistent attention to the major semantics variation than Eq. (6). Meanwhile, since we use CLIP as encoders rather than random sampling, our metric mitigates the bias in GT data, enabling a convenient comparison across different datasets. As shown in Fig. 1, our  $SSD$  indeed reflects better text-image consistency than the other metrics.

## Parallel Deep Fusion GAN

In this section, we propose the Parallel Deep Fusion Generative Adversarial Networks (PDF-GAN) equipped with Hard-negative Sentence Constructor (HNSC) and Semantic Projection (SProj). PDF-GAN fuses semantic information at different levels by using Parallel Fusion Modules (PFM). For semantic supervision, global and local discriminators, semantic perceptual losses, and a contrastive loss are adopted. To capture semantic information in texts more precisely and robustly, HNSC creates stable and controllable hard negative samples, and SProj can overcome the semantic gap by constraining the semantic optimization direction.

**Parallel Fusion** In our model, CLIP is used as an encoder to map images and texts into a joint semantic space. Guided by  $SSD$ , we confirm that using textual data at different levels improves text-image consistency. Global-level feature  $\{e_g\}^1$  is the caption embedding. Local-level features  $\{e_l\}^n$  are Aspects embeddings which are  $n$  key phrases extracted from the caption (Ruan et al. 2021). For example, ‘this black bird has yellow eyes and a long neck’, its aspects  $\{a\}^{n=3}$  are [‘this black bird’, ‘yellow eyes’, ‘long neck’]. Conditioned by  $\{e_g\}^1$  and  $\{e_l\}^n$ , the generation process is  $x_f = G(z | \{e_g\}^1, \{e_l\}^n)$  ( $G(z)$  for short), where  $z \sim N(0, 1)$  is a given noise and  $x_f$  is the generated image.

In Generator  $G$ , we propose PFM for efficient fusion between global and local features. PFM takes the output from previous steps as inputs and  $\{e_g\}^1$  and  $\{e_l\}^n$  as conditions (in Fig. 4 (c)). The input  $h_{t-1}$  is first upsampled to  $h'_{t-1}$ , then deep fusion (DF) is conducted on two groups of conditions. After DF, fused features from two branches are concatenated by channels and then go through a convolution layer and outputted as  $h_t$ . Especially for the Local

DF branch in Fig. 4 (b), we modify the Fusion Block from DF-GAN (Tao et al. 2020) to take local features. In Fig. 4 (a), two groups of MLPs learn the scale and the bias conditioned by local semantics, respectively. Input  $h_{t-1}$  is first expanded to the proper shape, then scaled and biased. The conditioned features are averaged and passed to later processors. Using PFM to fuse multiple levels of textual information efficiently, our PDF-GAN capture precise semantics while maintaining decent image quality. We use two PFMs in our experiments due to memory limitations.

**Hard-negative Sentence Constructor** HNSC constructs hard negative sentence samples by randomly replacing tokens in the given description according to the Part of Speech (POS). Nouns, verbs, and adjectives are replaced by other nouns, verbs, and adjectives. For example, for the text ‘this bird is blue on its tail and has a long pointy beak,’ our HNSC will randomly replace a certain percentage of words by its POS, (change ‘blue’ to ‘red,’ ‘tail’ to ‘head,’ etc.). Candidates for replacement are gathered from the dataset. HNSC produces stable and controllable hard negative textual samples which force discriminators to learn precise semantics.

**Training Objectives** We adopt the hinge loss (Zhang et al. 2019) for Discriminator  $D$  and Generator  $G$ .  $D$  usually takes four kinds of pairs: fake image with real text ( $G(z), e$ ), real image with real text ( $x, e$ ), fake image with mismatched text ( $G(z), e_m$ ) and real image with mismatched text ( $x, e_m$ ). To capture semantic information at the global and local levels, we use two discriminators  $D_g$  and  $D_l$ . For each  $D$  given by matched  $k$  conditions  $\{e\}^k$ , and mismatched  $k$  conditions  $\{e_m\}^k$ , the loss with modified Matching Aware Gradient Penalty (Tao et al. 2020) is defined as:

$$\begin{aligned} \mathcal{L}_D = & \mathbb{E}_{x_r \sim \mathbb{P}_r, e \in \{e\}^k} [1 - D_g(x, e)] \\ & + \frac{1}{2} [\mathbb{E}_{x_r \sim \mathbb{P}_r, e_m \in \{e_m\}^k} [1 + D_g(x, e_m)] \\ & + \mathbb{E}_{G(z) \sim \mathbb{P}_g, e \in \{e\}^k} [1 + D_g(G(z), e)] \\ & + q \mathbb{E}_{x \sim \mathbb{P}_r} [(\|\nabla_x D_g(x, \bar{e})\| + \|\nabla_e D(x, \bar{e})\|)^p]. \end{aligned} \quad (7)$$

The penalized term uses averaged  $\{e\}^k$  as the condition. Loss functions for  $D_g$  and  $D_l$  both follow Eq. (7) with that the given conditions  $\{e\}^k$  and  $\{e_m\}^k$  are global level  $\{e_g\}^1, \{e_{mg}\}^1$  and local level  $\{e_l\}^n, \{e_{ml}\}^n$ , respectively. Notice that  $\{e_{mg}\}^1$  is hard-negative sentence constructed by HNSC and  $\{e_{ml}\}^n$  are mismatched aspects from the batch.  $q$  and  $p$  are hyper-parameters set to 2.0 and 6 in our experiments. The adversarial loss of  $G$  is defined as:

$$\begin{aligned} \mathcal{L}_a = & -\mathbb{E}_{G(z) \sim \mathbb{P}_g} [D_g(G(z), \{e_g\}^1)] \\ & -\mathbb{E}_{G(z) \sim \mathbb{P}_g} [D_l(G(z), \{e_l\}^n)]. \end{aligned} \quad (8)$$

To enhance semantic information at different levels in  $G$ , we adopt global and local semantic perceptual losses  $\mathcal{L}_g, \mathcal{L}_l$ :

$$\mathcal{L}_g = f_C(G(\tilde{z}))^T \cdot \tilde{e}_g, \mathcal{L}_l = \frac{1}{n} \sum_{i=1}^n f_C(G(\tilde{z}))^T \cdot \tilde{e}_l^i. \quad (9)$$

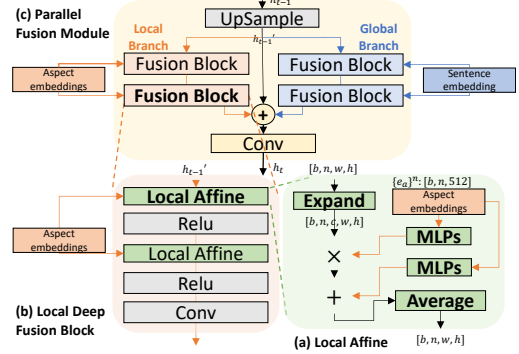


Figure 4: Parallel Fusion Module

#### Algorithm 1: Semantic Projection in One Step

**Require:** Training data  $(\{e_g\}^1, \{e_l\}^n)$ , Generator  $G$ , Discriminators  $D_g, D_l, z \sim N(0, 1)$

- 1:  $x' = G(z \mid \{e_g\}^1, \{e_l\}^n)$
- 2:  $y'_g = D_g(x' \mid \{e_g\}^1), y'_l = D_l(x' \mid \{e_l\}^n)$
- 3: Calculate loss  $\mathcal{L}_{D_g}, \mathcal{L}_{D_l}$  for  $D_g, D_l$   $\triangleright$  See Eq. (7).
- 4:  $\delta_{D_g} \leftarrow \nabla \mathcal{L}_{D_g}, \delta_{D_l} \leftarrow \nabla \mathcal{L}_{D_l}$
- 5:  $\theta_{D_g} \leftarrow \theta - \alpha \delta_{D_g}, \theta_{D_l} \leftarrow \theta - \alpha \delta_{D_l}$
- 6: Calculate  $\mathcal{L}_a, \mathcal{L}_s$   $\triangleright$  See Eq. (11).
- 7:  $\delta_a \leftarrow \nabla \mathcal{L}_a, \delta_s \leftarrow \nabla \mathcal{L}_s$
- 8:  $\bar{\delta}_s \leftarrow \text{PROJECT}(\delta_a, \delta_s)$   $\triangleright$  See Eq. (12).
- 9:  $\theta_G \leftarrow \theta_G - (\alpha_a \delta_a + \alpha_s \bar{\delta}_s)$

**Return:**  $x'$

A contrastive loss  $\mathcal{L}_c$  is introduced to further repel mismatched samples:

$$\mathcal{L}_c = \frac{f_C(G(\tilde{z}))^T \cdot \tilde{e}_{mg}}{f_C(G(\tilde{z}))^T \cdot \tilde{e}_{mg} + f_C(G(\tilde{z}))^T \cdot \tilde{e}_g}. \quad (10)$$

The final generative loss  $\mathcal{L}_G$  combines above four losses:

$$\mathcal{L}_G = \underbrace{\lambda(\mathcal{L}_g + \mathcal{L}_l + \mathcal{L}_c)}_{\text{Semantic loss } \mathcal{L}_s} + \underbrace{\mathcal{L}_a}_{\text{Adversarial loss}} \quad (11)$$

where we set  $\lambda = 10$  empirically in our experiments. Sensitivity analysis is provided in our supplementary material S3.

**Semantic Projection** Since the semantic gap in CLIP space causes conflicts in optimization directions between  $\mathcal{L}_a$  and  $\mathcal{L}_s$ , we design SProj to overcome the conflicts.

Inspired by GEM for continuous learning (Lopez-Paz and Ranzato 2017), we treat minimizing  $\mathcal{L}_a$  and  $\mathcal{L}_s$  as two tasks. Instead of training on two tasks alternately, we optimize them simultaneously. Algorithm 1 shows the training and protocol of SProj in one step. In each step, after we calculate the gradients  $\delta_a, \delta_s$  for  $\mathcal{L}_a$  and  $\mathcal{L}_s$ , we conduct *PROJECT* on  $\delta_s$  before we process backpropagation on both tasks. If there is a direction conflict, the semantic optimization direction  $\delta_s$  will be re-projected to a new direction  $\bar{\delta}_s$  in which it can optimize for  $\mathcal{L}_s$  while not enlarging  $\mathcal{L}_a$ . *PROJECT* is defined as: For gradients  $\Delta := -(\delta_a, \delta_s)$ , if  $\langle \delta_a, \delta_s \rangle \geq 0$ , we need

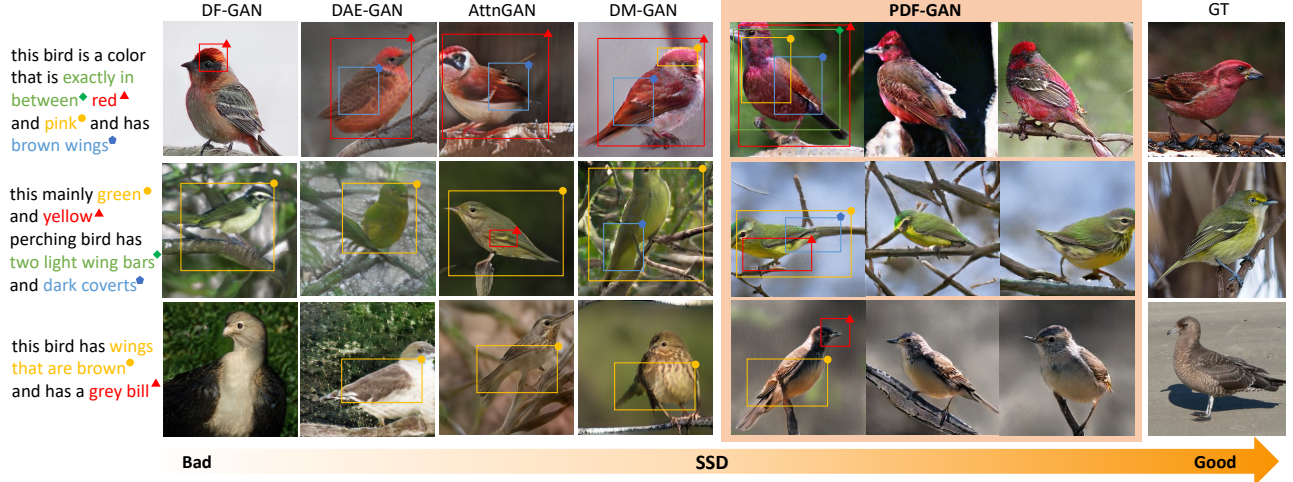


Figure 5: Examples for T2I synthesis by AttnGAN, DM-GAN, DAE-GAN, DF-GAN and our PDF-GAN on CUB.

CUB	$SSD \downarrow$	$CS \uparrow$	$R \uparrow$	$CFID \downarrow$
GT	72.07	69.83	21.26	0.00
AttnGAN	76.10	68.00	67.82	6.89
DM-GAN	75.51	69.03	72.31	<b>3.04</b>
DAE-GAN	76.61	68.93	<b>85.45</b>	4.16
DF-GAN	76.82	67.80	39.50	4.55
<b>PDF-GAN</b>	<b>72.72</b>	<b>80.28</b>	11.75	12.86
COCO	$SSD$	$CS$	$R$	$CFID$
GT	72.68	68.30	69.26	0.00
AttnGAN	88.01	50.48	85.47	7.75
DM-GAN	86.62	51.10	88.56	<b>6.25</b>
DAE-GAN	87.98	51.88	<b>92.61</b>	17.11
DF-GAN	82.67	60.85	51.75	7.43
<b>PDF-GAN</b>	<b>76.49</b>	<b>72.98</b>	49.79	8.68

Table 1: Text-image consistency results of  $SSD$ ,  $CS$ ,  $R$  and  $CFID$  on CUB and COCO. Best results are highlighted.

solve the Quadratic Program to get solution  $\vartheta^*$  for  $\vartheta$ :

$$\min_{\vartheta} 1/2 [\vartheta^T \Delta \Delta^T + \delta_s^T \Delta^T \vartheta], \quad s.t. \quad \vartheta \geq 0. \quad (12)$$

The projected gradients can then be updated as  $\hat{\delta} = G^T \vartheta^* + g_s$ . With SProj, the model can converge to the closest point between texts and image features in the semantic space (as shown in Fig. 2 (a)), attaining a mutual balance between text-image consistency and image quality.

## Experiments

**Experimental Setup** In our experiments, we evaluate our metric and method on two datasets, CUB (Wah et al. 2011) and COCO (Lin et al. 2014). The generated images are judged by both text-image consistency metrics and image quality metrics. For qualitatively evaluating the text-image consistency, the proposed  $SSD$  is used and compared with other popular metrics  $R$  (Xu et al. 2018),  $CS$  (Hessel et al. 2021), and  $CFID$  (Soloveitchik et al. 2021). For a fair comparison,  $CFID$  is calculated from CLIP embeddings, and all

	<b>CUB</b>		<b>COCO</b>
	$IS \uparrow$	$FID \downarrow$	$FID \downarrow$
AttnGAN	4.36	23.98	35.49
DM-GAN	4.75	16.09	32.64
DAE-GAN	4.42	15.19	28.12
MirrorGAN	4.56	18.34	34.71
SD-GAN	4.67	-	-
TIME	<u>4.91</u>	<u>14.30</u>	34.14
DF-GAN	<b>5.10</b>	14.81	<b>19.32</b>
<b>PDF-GAN</b>	4.59	<b>12.30</b>	<u>22.94</u>

Table 2: Image quality results of  $IS$  on CUB and  $FID$  on CUB and COCO. Best and second best results are highlighted as **bold** and by underlines, respectively.

CLIP-based metrics,  $SSD$ ,  $CS$  and  $CFID$ , are scaled by 100 in our experiment. The standard metrics, Inception Score (IS) (Salimans et al. 2016) and Fréchet Inception Distance (FID) (Heusel et al. 2017), are used to quantitatively evaluate the generated image quality. IS was not used to evaluate COCO because it works not well on COCO as indicated in (Tao et al. 2020; Zhang and Schomaker 2021).

All the metrics are computed over 30K generated images. We use the released models from competitors for the metric calculation of text-image consistency, and directly adopt their reported image quality results. The number of the aspect per caption is set to 3, and the maximum number of words per caption is set to 18. More training details and model parameter settings are in our supplementary material S2. Our code will be released XXXX.

**Appraise SSD** We appraise our  $SSD$  by comparing it with  $CS$ ,  $R$  and  $CFID$  on AttnGAN (Xu et al. 2018), DM-GAN (Zhu et al. 2019), DAE-GAN (Ruan et al. 2021), DF-GAN (Tao et al. 2020) and our PDF-GAN. Quantitative results are presented in Table 1, and the generated examples are visualized in Figs. 5-6.

As shown in Table 1,  $R$ 's indirect measurement and highly-dataset biased sampling generate even better scores

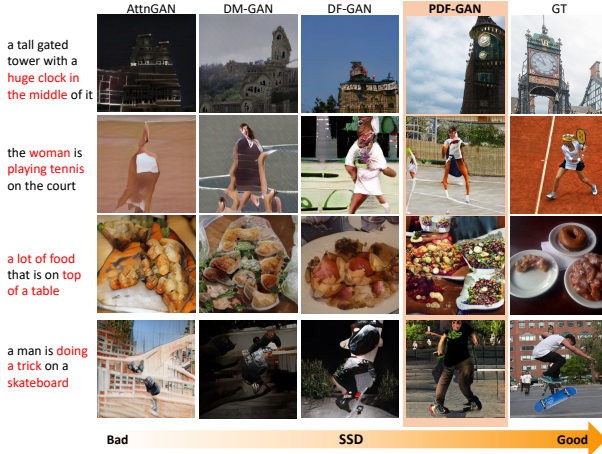


Figure 6: Examples for T2I synthesis by AttnGAN, DM-GAN, DF-GAN and our PDF-GAN on COCO.

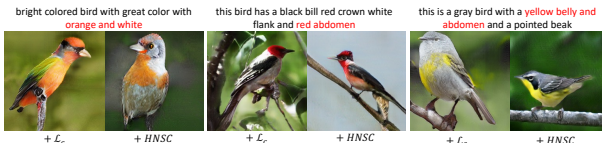


Figure 7: Examples generated by ablation task  $+L_c$  (CS: 71.76,  $SSD$ : 74.49) and  $+HNSC$  (CS: 71.08,  $SSD$ : 73.68).

for most methods than GT, indicating its severe limitations. Leveraging CLIP embeddings, CS can better reflect text-image consistency. However, since CLIP may suffer from binding attributes to objects (Ramesh et al. 2022), CS struggles to reflect precise semantics consistency. E.g., it might lead that our PDF-GAN exceeds GT in CS. Such drawback of CS can also be seen in Fig. 7 from our ablation studies, where the model failing to capture precise semantics like ‘orange and white’ but obtains higher CS.

CFID aims to measure the distance between images’ distributions approximately. If we compare the CFID scores in Table 1 with the corresponding examples in Fig. 5, Fig. 6, it is evident that CFID is not in line with the consistency. This is mainly because real images usually contain redundancies not mentioned by texts which may however be not reacquired in the generated images, causing unsuitable fist-moment term in Eq. (6).

Our  $SSD$  mitigates the drawbacks of both CS and CFID. As shown in Fig. 5 and Fig. 6 that are organized in  $SSD$  descending-order horizontally, text-image consistency can indeed be observed better from left to right. In contrast to CS in Fig. 7, our  $SSD$  demonstrates clearly better semantic consistency. Furthermore, since our  $SSD$  alleviates the dataset bias, we can compare  $SSD$  across different datasets. See more analysis in our supplementary material S1.

**Appraise PDF-GAN** If we examine  $SSD$  scores in Table 1, all the methods show better text-image consistency on CUB than that on COCO, while our PDF-GAN achieves the best text-image consistency. Meanwhile, PDF-GAN can

Task	$SSD \downarrow$	$CS \uparrow$	$IS \uparrow$	$FID \downarrow$
Baseline	76.63	59.94	4.50	24.16
$+ L_g$	75.59	68.10	4.63	14.69
$+ SProj$	74.10	70.70	<b>4.81</b>	15.55
$+ L_c$	74.49	71.76	4.58	14.78
$+ HNSC$	73.68	71.03	4.61	14.41
<b>+ PFM (PDF-GAN)</b>	<b>72.72</b>	<b>73.63</b>	4.59	<b>12.30</b>

Table 3: Ablation study of different components on CUB.

maintain decent image quality, achieving the best (12.30) and second best (22.94) in FID on CUB and COCO.

As shown in Figs. 5-6, PDF-GAN can capture complex and precise semantics while maintaining decent quality. For a less complex dataset like CUB, our PDF-GAN surpasses 2.80 in  $SSD$  over the second best method while DF-GAN produces high-quality but text-mismatched images; other attention-based methods fail to capture detailed semantics. Moreover, PDF-GAN can stably generate complex semantics in visual (e.g. in Fig. 5 where the bird matches ‘exactly in red and pink’ and other highlighted phrases). The superiority of our PDF-GAN is more evident on COCO. In comparison, DF-GAN has more balanced results on both datasets and may also produce high-quality images, but the overall text-image consistency is not promising. Our proposed PDF-GAN can capture the complex semantics and have 6.18 improvement in  $SSD$  on COCO, suggesting our model is able to capture complex semantics (see Fig. 6). More generated examples of PDF-GAN can be seen in the supplementary material S4.

**Ablation Study** We take CUB as one typical example for ablative analysis. These results can be seen in Table 3 whilst examples are shown in Fig. 2 (b). Two findings are verified: 1) The semantic gap can cause optimization conflicts between adversarial and semantic losses. 2) Using random samples from the dataset or the training batch may prevent discriminators from learning precise semantics. Overall, these two issues could be well tackled by the proposed SProj and HNSC.

Reported in the first group of experiment of Table 3, brutally adding semantic perceptual loss can improve image quality, but may not significantly improve text-image consistency due to the semantic gap. SProj can strengthen the  $L_g$ ’s supervision, forcing the model to be further optimized in semantics without sacrificing the image quality. As shown in Fig. 2 (b)(2), SProj with semantic perceptual loss benefits capturing more semantic details.

The second group shows that contrastive loss  $L_c$  may deteriorate text-image consistency if random mismatched texts are given. The scores of  $SSD$  and IS get worse when this loss is added. However, HNSC can mitigate this issue by offering stable and controllable hard-negative sentences as mismatched samples. It pushes the discriminators to learn more semantic differences between positive and hard negative texts, thus improving the model’s capability in capturing precise semantics, as seen in Fig. 2 (b)(3) and Fig. 7. It also eases the degradation in IS and improves FID.

## Conclusion

In this paper, we propose a novel metric *SSD* to better evaluate text-image consistency. Both theoretical analysis and empirical investigation show that *SSD* can indeed reflect the semantic consistency in text-to-image generation. We also design a novel framework called PDF-GAN along with two plug-and-play modules that can further enhance the text-image consistency. Experiments on benchmark datasets confirm the effectiveness of *SSD* as well as the advantages of PDF-GAN both qualitatively and quantitatively.

## References

Bodla, N.; Hua, G.; and Chellappa, R. 2018. Semi-supervised FusedGAN for conditional image generation. In *Proceedings of the European Conference on Computer Vision (ECCV)*, 669–683.

Brock, A.; Donahue, J.; and Simonyan, K. 2018. Large scale GAN training for high fidelity natural image synthesis. *arXiv preprint arXiv:1809.11096*.

Cha, M.; Gwon, Y. L.; and Kung, H. 2019. Adversarial learning of semantic relevance in text to image synthesis. In *Proceedings of the AAAI conference on artificial intelligence*, volume 33, 3272–3279.

Cheng, J.; Wu, F.; Tian, Y.; Wang, L.; and Tao, D. 2020. RiFeGAN: Rich feature generation for text-to-image synthesis from prior knowledge. In *Proceedings of the IEEE/CVF Conference on Computer Vision and Pattern Recognition*, 10911–10920.

Gal, R.; Patashnik, O.; Maron, H.; Chechik, G.; and Cohen-Or, D. 2021. Stylegan-nada: Clip-guided domain adaptation of image generators. *arXiv preprint arXiv:2108.00946*.

Gao, L.; Chen, D.; Song, J.; Xu, X.; Zhang, D.; and Shen, H. T. 2019. Perceptual pyramid adversarial networks for text-to-image synthesis. In *Proceedings of the AAAI Conference on Artificial Intelligence*, volume 33, 8312–8319.

Gou, Y.; Wu, Q.; Li, M.; Gong, B.; and Han, M. 2020. SegAttnGAN: Text to image generation with segmentation attention. *arXiv preprint arXiv:2005.12444*.

Hessel, J.; Holtzman, A.; Forbes, M.; Bras, R. L.; and Choi, Y. 2021. Clipscore: A reference-free evaluation metric for image captioning. *arXiv preprint arXiv:2104.08718*.

Heusel, M.; Ramsauer, H.; Unterthiner, T.; Nessler, B.; and Hochreiter, S. 2017. Gans trained by a two time-scale update rule converge to a local nash equilibrium. *Advances in neural information processing systems*, 30.

Hinz, T.; Heinrich, S.; and Wermter, S. 2020. Semantic object accuracy for generative text-to-image synthesis. *IEEE transactions on pattern analysis and machine intelligence*.

Hong, S.; Yang, D.; Choi, J.; and Lee, H. 2018. Inferring semantic layout for hierarchical text-to-image synthesis. In *Proceedings of the IEEE conference on computer vision and pattern recognition*, 7986–7994.

Huang, W.; Da Xu, R. Y.; and Oppermann, I. 2019. Realistic image generation using region-phrase attention. In *Asian Conference on Machine Learning*, 284–299. PMLR.

Huang, X.; Wang, M.; and Gong, M. 2019. Hierarchically-fused generative adversarial network for text to realistic image synthesis. In *2019 16th Conference on Computer and Robot Vision (CRV)*, 73–80. IEEE.

Kay, S. M. 1993. *Fundamentals of statistical signal processing: estimation theory*. Prentice-Hall, Inc.

Li, B.; Qi, X.; Lukasiewicz, T.; and Torr, P. 2019. Controllable text-to-image generation. *Advances in Neural Information Processing Systems*, 32.

Li, R.; Wang, N.; Feng, F.; Zhang, G.; and Wang, X. 2020. Exploring global and local linguistic representations for text-to-image synthesis. *IEEE Transactions on Multimedia*, 22(12): 3075–3087.

Lin, T.-Y.; Maire, M.; Belongie, S.; Hays, J.; Perona, P.; Ramanan, D.; Dollár, P.; and Zitnick, C. L. 2014. Microsoft coco: Common objects in context. In *European conference on computer vision*, 740–755. Springer.

Lopez-Paz, D.; and Ranzato, M. 2017. Gradient episodic memory for continual learning. *Advances in neural information processing systems*, 30.

Ma, J.; Zhang, L.; and Zhang, J. 2019. SD-GAN: Saliency-discriminated GAN for remote sensing image superresolution. *IEEE Geoscience and Remote Sensing Letters*, 17(11): 1973–1977.

Qiao, T.; Zhang, J.; Xu, D.; and Tao, D. 2019. Mirrorgan: Learning text-to-image generation by redescription. In *Proceedings of the IEEE/CVF Conference on Computer Vision and Pattern Recognition*, 1505–1514.

Radford, A.; Kim, J. W.; Hallacy, C.; Ramesh, A.; Goh, G.; Agarwal, S.; Sastry, G.; Askell, A.; Mishkin, P.; Clark, J.; et al. 2021. Learning transferable visual models from natural language supervision. In *International Conference on Machine Learning*, 8748–8763. PMLR.

Ramesh, A.; Dhariwal, P.; Nichol, A.; Chu, C.; and Chen, M. 2022. Hierarchical text-conditional image generation with clip latents. *arXiv preprint arXiv:2204.06125*.

Ramesh, A.; Pavlov, M.; Goh, G.; Gray, S.; Voss, C.; Radford, A.; Chen, M.; and Sutskever, I. 2021. Zero-shot text-to-image generation. In *International Conference on Machine Learning*, 8821–8831. PMLR.

Reed, S.; Akata, Z.; Yan, X.; Logeswaran, L.; Schiele, B.; and Lee, H. 2016. Generative adversarial text to image synthesis. In *International conference on machine learning*, 1060–1069. PMLR.

Ruan, S.; Zhang, Y.; Zhang, K.; Fan, Y.; Tang, F.; Liu, Q.; and Chen, E. 2021. Dae-gan: Dynamic aspect-aware gan for text-to-image synthesis. In *Proceedings of the IEEE/CVF International Conference on Computer Vision*, 13960–13969.

Salimans, T.; Goodfellow, I.; Zaremba, W.; Cheung, V.; Radford, A.; and Chen, X. 2016. Improved techniques for training gans. *Advances in neural information processing systems*, 29.

Seshadri, A. D.; and Ravindran, B. 2021. Multi-Tailed, Multi-Headed, Spatial Dynamic Memory refined Text-to-Image Synthesis. *arXiv preprint arXiv:2110.08143*.

Soloveitchik, M.; Diskin, T.; Morin, E.; and Wiesel, A. 2021. Conditional frechet inception distance. *arXiv preprint arXiv:2103.11521*.

Tan, H.; Liu, X.; Li, X.; Zhang, Y.; and Yin, B. 2019. Semantics-enhanced adversarial nets for text-to-image synthesis. In *Proceedings of the IEEE/CVF International Conference on Computer Vision*, 10501–10510.

Tao, M.; Tang, H.; Wu, S.; Sebe, N.; Jing, X.-Y.; Wu, F.; and Bao, B. 2020. Df-gan: Deep fusion generative adversarial networks for text-to-image synthesis. *arXiv preprint arXiv:2008.05865*.

Wah, C.; Branson, S.; Welinder, P.; Perona, P.; and Belongie, S. 2011. The caltech-ucsd birds-200-2011 dataset.

Wang, M.; Lang, C.; Feng, S.; Wang, T.; Jin, Y.; and Li, Y. 2021. Text to photo-realistic image synthesis via chained deep recurrent generative adversarial network. *Journal of Visual Communication and Image Representation*, 74: 102955.

Wang, Z.; Liu, W.; He, Q.; Wu, X.; and Yi, Z. 2022. CLIP-GEN: Language-Free Training of a Text-to-Image Generator with CLIP. *arXiv preprint arXiv:2203.00386*.

Xu, T.; Zhang, P.; Huang, Q.; Zhang, H.; Gan, Z.; Huang, X.; and He, X. 2018. AttnGAN: Fine-grained text to image generation with attentional generative adversarial networks. In *Proceedings of the IEEE conference on computer vision and pattern recognition*, 1316–1324.

Yuan, M.; and Peng, Y. 2019. Ckd: Cross-task knowledge distillation for text-to-image synthesis. *IEEE Transactions on Multimedia*, 22(8): 1955–1968.

Zhang, H.; Goodfellow, I.; Metaxas, D.; and Odena, A. 2019. Self-attention generative adversarial networks. In *International conference on machine learning*, 7354–7363. PMLR.

Zhang, H.; Koh, J. Y.; Baldridge, J.; Lee, H.; and Yang, Y. 2021. Cross-modal contrastive learning for text-to-image generation. In *Proceedings of the IEEE/CVF Conference on Computer Vision and Pattern Recognition*, 833–842.

Zhang, H.; Xu, T.; Li, H.; Zhang, S.; Wang, X.; Huang, X.; and Metaxas, D. N. 2017. Stackgan: Text to photo-realistic image synthesis with stacked generative adversarial networks. In *Proceedings of the IEEE international conference on computer vision*, 5907–5915.

Zhang, H.; Xu, T.; Li, H.; Zhang, S.; Wang, X.; Huang, X.; and Metaxas, D. N. 2018. Stackgan++: Realistic image synthesis with stacked generative adversarial networks. *IEEE transactions on pattern analysis and machine intelligence*, 41(8): 1947–1962.

Zhang, Z.; and Schomaker, L. 2021. DTGAN: Dual attention generative adversarial networks for text-to-image generation. In *2021 International Joint Conference on Neural Networks (IJCNN)*, 1–8. IEEE.

Zhang, Z.; Xie, Y.; and Yang, L. 2018. Photographic text-to-image synthesis with a hierarchically-nested adversarial network. In *Proceedings of the IEEE conference on computer vision and pattern recognition*, 6199–6208.

Zhu, M.; Pan, P.; Chen, W.; and Yang, Y. 2019. Dm-gan: Dynamic memory generative adversarial networks for text-to-image synthesis. In *Proceedings of the IEEE/CVF Conference on Computer Vision and Pattern Recognition*, 5802–5810.